THE JOURNAL OF PHYSICAL CHEMISTRY B

Article

Molecular Dynamics Simulation of the Early Stages of the Synthesis of Periodic Mesoporous Silica

Miguel Jorge, Jose# R. B. Gomes, M. Natália D. S. Cordeiro, and Nigel A. Seaton

J. Phys. Chem. B, **2009**, 113 (3), 708-718 • DOI: 10.1021/jp806686w • Publication Date (Web): 31 December 2008

Molecular Dynamics Simulation of the Early Stages of the Synthesis of Periodic Mesoporous Silica

Miguel Jorge,*,† José R. B. Gomes,‡ M. Natália D. S. Cordeiro,§ and Nigel A. Seaton||

Laboratory of Separation and Reaction Engineering (LSRE), Faculdade de Engenharia, Universidade do Porto, Rua Dr. Roberto Frias, s/n, 4200-465 Porto, Portugal; CICECO, Campus Universitário de Santiago, Universidade de Aveiro, 3810-193 Aveiro, Portugal; REQUIMTE, Faculdade de Ciências, Universidade do Porto, Rua do Campo Alegre 687, 4169-007 Porto, Portugal; and Institute for Materials and Processes, School of Engineering and Electronics, University of Edinburgh, King's Buildings, Mayfield Road, Edinburgh EH9 3JL, U.K.

Received: July 28, 2008; Revised Manuscript Received: October 28, 2008

We present results of detailed atomistic modeling of the early stages of the synthesis of periodic mesoporous silica using molecular dynamics. Our simulations lead to the proposal of a mechanism that validates several previous experimental and modeling studies and answers many controversial issues regarding the synthesis of mesoporous silicas. In particular, we show that anionic silicates interact very strongly with cationic surfactants and significantly adsorb on the surface of micelles, displacing a fraction of previously bound bromide counterions. This induces an increase in micelle size and also enhances silica condensation at the micelle surface. The presence of larger silica aggregates in solution further promotes the growth of micelles and, by binding to surfactant molecules in different micelles, their aggregation. This work demonstrates the crucial role played by silica in influencing, by way of a cooperative templating mechanism, the structure of the eventual liquid-crystal phase, which in turn determines the structure of the porous material.

1. Introduction

Since their discovery in the early 1990s,[1] surfactant-templated periodic mesoporous silica (PMS) materials have attracted a great deal of interest in the scientific community. This stems mainly from their wide variety of applications, which range from adsorption to drug delivery, including catalysis, host−guest chemistry, membrane separation, optical and electrical applications, and nanocomposites.[2,3] PMS materials are synthesized from an aqueous solution of surfactants and a silica source, in which the surfactant molecules self-assemble into a liquid-crystal phase that serves as a template around which the silica scaffold forms. After condensation of the silica scaffold, the surfactant is removed, usually by calcination, leaving a porous material with amorphous walls and a pore network that is closely related to the morphology of the liquid-crystal mesophase.[2] The nature of this templated synthesis process suggests the possibility of tuning properties such as the pore size, geometry, and surface chemistry to a particular application by controlling the synthesis conditions. However, success of this a priori design strategy relies on a detailed understanding of the synthesis process of templated materials, which is still lacking. In fact, many independent studies yield seemingly conflicting information, and despite the multitude of proposed mechanistic pathways, none has emerged as a uniquely accepted answer to the problem.

The first attempts to elucidate the synthesis mechanism of PMS materials were based on experimental characterization of the resulting solid phase, using techniques such as X-ray diffraction[1,4−7] (XRD), transmission electron microscopy[1,4−6] (TEM), infrared and Raman spectroscopy,[4,6] solid-state NMR,[1,4,6,7] temperature-programmed desorption[4,7] (TPD), and gas adsorption.[1,4,6] Mechanistic pathways were inferred from only indirect evidence by testing different initial synthesis conditions and relating these to the final solid structure. Using this strategy, Beck et al.[1] suggested two alternative generic mechanisms for PMS synthesis from solutions of cationic surfactants and anionic silicates. The first of these is the so-called liquid-crystal templating (LCT) mechanism, in which silica condenses around a preformed stable surfactant liquid-crystal phase. The second mechanism, the so-called cooperative templating (CT) mechanism, proposes that it is the silicate species themselves that promote the formation of the liquid-crystal template, by changing the nature of the phase equilibrium. The resulting mesophase has thus been termed a "silicatropic" liquid crystal.[8] In the aforementioned studies, PMS materials were synthesized from solutions with surfactant concentrations that were too low to allow for the observation of a pre-existing liquid-crystal phase,[9] indicating that the governing mechanism obeyed the CT pathway. However, later studies have suggested that, under certain conditions, PMS materials may also be formed by a true LCT pathway.[10] The two mechanisms represent two fundamentally different views of the synthesis process: structure directing by the surfactant phase, with silica playing only a minor role, versus templating in which silica plays a major role in directing the final structure.

Attempts to explain the CT mechanism in more detail quickly followed. Monnier et al.[5] proposed a mechanism consisting of three crucial stages: (i) multidentate binding of oligomeric silicates at the surface of pre-existing surfactant micelles; (ii) preferred silica condensation at the micelle surface, caused by a significant increase in the local silica concentration; (iii) charge density matching between silicates and surfactants, dictating the final structure of the mesophase. These concepts were later explored by Huo et al.,[7] who was able to synthesize periodic

* Corresponding author. E-mail: mjorge@fe.up.pt.
† Faculdade de Engenharia, Universidade do Porto.
‡ Universidade de Aveiro.
§ Faculdade de Ciências, Universidade do Porto.
|| University of Edinburgh.

10.1021/jp806686w CCC: $40.75
Published on Web 12/31/2008

mesoporous materials using different inorganic species under a wide range of conditions. These authors also suggested the possibility that the inorganic ions might interact preferentially with free surfactant monomers rather than with micelles. The growth of the silica/surfactant phase would then proceed at the expense of pre-existing micelles, whose presence in the initial solution was not considered essential for the formation of a silicatropic mesostructure.[7] Once again, two distinct views were put forth to explain the way in which silicates direct the formation of silica/surfactant mesophases: interaction with pre-existing micelles versus interaction with free surfactant molecules. The fact that only indirect experimental information on PMS synthesis was available at the time (up to 1994) meant that this issue remained unresolved.

The subsequent development of experimental techniques prompted several in situ studies of PMS synthesis solutions. Using solution NMR, small-angle XRD, and polarized optical microscopy, Firouzi et al.[8,11] focused on high-pH systems in which silica condensation was suppressed. They were able to show that addition of silica caused phase separation into a dilute solution composed of surfactant micelles and small silicates, and a concentrated phase consisting of a surfactant liquid crystal surrounded by multiply charged silica cubic octamers. They proposed that the formation of the liquid-crystal phase begins with the exchange of halide counterions by cubic octamers at the micelle surface. The cubic octamers are able to bind to more than one surfactant molecule, thus promoting micelle elongation and intermicellar aggregation to yield a hexagonal silicatropic liquid crystal.

The work of Firouzi et al.[8,11] provided the first explanation of the CT mechanism based on in situ evidence, but many aspects remained contentious. For instance, the ability of silicates to induce a sphere-to-rod transition in aqueous cationic surfactant solutions was demonstrated by Lee et al.[12] and by Albuquerque et al.[13] The latter also observed that silicates were able to promote the formation of a hexagonal liquid crystal. However, in their fluorescence quenching studies, Zana and co-workers[14,15] did not observe any significant change in micelle size on addition of silicates, even when these were in the form of cubic octamers.[15] Using cryo-TEM, Regev[16] observed a sphere-to-rod transition upon addition of silica, eventually leading to the formation of clusters of cylindrical micelles. On the other hand, Galarneau et al.[17] concluded that silicates promoted the formation of irregular aggregates of spherical micelles. They suggested that a gradual transition from spheres to cylinders took place within those aggregates by an Ostwald ripening process, eventually forming a hexagonal liquid crystal. This scenario was supported by Sadasivan et al.[18] and Beurroies et al.,[19] who argued for a phase transition between disordered micellar aggregates and an ordered liquid crystal.

Another widely debated aspect is whether silicatropic phases are induced by silica adsorption onto micelles or by association of silicates with free surfactants. Zana and co-workers[14,15] observed that only a small proportion of bromide counterions were displaced from micelles upon addition of anionic silica to the system. Thus, they concluded that silicates do not replace bromide at the micelle surface but rather interact with free surfactants forming silica/surfactant complexes that then grow at the expense of micelles, in a mechanism similar to that proposed by Huo et al.[7] In a recent paper, Vautier-Giongo and Pastore[20] have observed that about 30−40% of bromide ions are exchanged for silicates at the micelle surface when silica is added to a micellar solution. Using in situ electron paramagnetic resonance spectroscopy, Zhang et al.[21−23] identified two distinct stages in PMS synthesis: a fast stage attributed to oligomeric silica interacting with surfactants and inducing the formation of a liquid crystal followed by a slow stage of silica condensation and dehydration. Although a strong silica−surfactant interaction was inferred, they could not specify whether this occurred at the micelle surface or with free surfactants. In a similar study, Galarneau et al.[17] concluded that silicates do replace bromide at the micelle surface, thus inducing micellar aggregation. In a recent study of a silica-bound spin probe, Baute et al.[24] observed a close interaction of silica with surfactant head groups at the surface of micelles, thus supporting the interpretation of Firouzi et al.[8,11] rather than that of Zana and co-workers.[14,15] Furthermore, those authors concluded that silica condensation initially pushed the spin-label away from the micelle surface into a highly fluid silica layer surrounding several micelles. Subsequent phase separation, condensation, and dehydration led to the formation of the solid material.[24]

What emerges from the above discussion is that, although our knowledge of the general aspects of PMS synthesis has improved significantly since the discovery of these materials, the mechanism by which silica and surfactant interact to form a silicatropic liquid crystal in the early stages of the process is still not known precisely.[25] Several questions remain unanswered: Do silicates play a dominant role in determining the mesophase structure? Are they responsible for changes in micelle size and shape? Do they promote intermicellar aggregation? If so, what is the physical mechanism? Do silicates adsorb on the surface of micelles, or do they preferentially interact with free surfactants? The difficulty in answering those questions is mostly due to the high complexity of the synthesis process, which depends on a delicate interplay between hydrophobic forces, electrostatic interactions, chemical reactions, and phase equilibrium. Thus, despite extensive efforts, it is extremely challenging to experimentally probe the crucial early stages of the synthesis at the molecular level, giving rise to the often conflicting views described above.

In this context, molecular simulation methods may be able to provide the missing link between microscopic phenomena and macroscopic observations. However, only a few attempts to approach this problem from a theoretical or computational standpoint have been reported.[26−33] Bhattacharya and Mahanti[26] performed off-lattice Monte Carlo simulations to study the self-assembly of a two-dimensional, coarse-grained, ionic surfactant model interacting by a Lennard-Jones potential and a screened Coulomb term. They studied the effect of several parameters, including the presence of neutral host particles, and concluded that the effect of inorganic particles on the micellar structure depended on the size, density, and interaction strength of the former. Because of the drastic simplifications introduced in the model, only general trends were discussed, and a direct comparison with PMS synthesis solutions was not attempted. Siperstein and Gubbins[27,28] calculated surfactant/inorganic/water phase diagrams using a three-dimensional lattice model and assuming a strong attraction between inorganic particles and surfactant head groups, but without accounting explicitly for silica condensation. They were able to see phase separation into a dilute and a concentrated phase, with the latter exhibiting mesostructures that were in good qualitative agreement with experimental observations.[28] Their model has been recently extended to study the formation of hybrid organic−inorganic materials.[29,30] The main limitation of this approach is the inability of the model to explain in detail the physics behind silica/surfactant interactions, relying instead on an assumed effective attraction between those species. An entirely different approach

was put forward by Schumacher et al.[31] Instead of attempting to describe the self-assembly of surfactants in the presence of silica, they simulated the condensation of silica around preformed micelles using a kinetic Monte Carlo procedure. The micelles were represented by smooth, uniform cylinders and were later removed to reproduce the calcination process. Their method generated structures that were realistic and were able to accurately model experimental adsorption isotherms on equivalent PMS materials. Once again, however, the model provided no insight into the physics of silica/surfactant interactions, relying on an assumed attraction between silicates and micelles. Finally, it is also worth mentioning the mean-field model developed by Gov et al.[32] By assuming that silicates cause a linear decrease in the effective surfactant head group area and promote intermicellar condensation, these authors were able to qualitatively explain many morphological transitions observed experimentally during PMS synthesis. This model presented only a phenomenological description of silica/surfactant interactions, accounting only implicitly for their effect.

Clearly, none of the theoretical approaches described in the previous paragraph are able to probe the specific interactions between silicates and surfactants, be it monomers or micelles, during the early stages of the reaction. In this work, our aim was to take advantage of recent improvements in computer power and in simulation methodology to perform a detailed study at the molecular level of the early stages of the PMS synthesis process. In a recent letter,[33] we presented the first explicit molecular dynamics (MD) simulations of surfactant self-assembly in the presence of silica using realistic atomistic models. Our results showed that anionic silicic acid monomers promote the formation of larger micelles relative to solutions containing only bromide counterions. In the present paper, we present a more detailed analysis of the self-assembly in the presence of silica monomers and go one step further by studying solutions with a distribution of silicate oligomers, representing a later stage in the reaction process. Furthermore, we analyze the possibility of exchange between bromide and silicate counterions at the micelle surface in an attempt to answer some of the outstanding questions about the mechanism of formation of silicatropic liquid-crystal phases.

2. Computational Methods

Simulations were carried out using the GROMACS 3.3 molecular dynamics package.[34,35] The equations of motion were integrated with the Verlet leapfrog algorithm[36] and a time step of 2 fs. The *NpT* ensemble was used for all runs, with the temperature fixed at 298.15 K by applying the Nosé-Hoover thermostat,[37,38] and the pressure was fixed at 1 bar by using the Parrinello-Rahman barostat.[39] The simulation boxes were always cubic, with periodic boundary conditions in all Cartesian directions. The total potential energy was calculated as the sum of harmonic angle bending terms, torsional terms of the Ryckaert−Bellemans form, Lennard-Jones 12−6 terms, and Coulomb electrostatic terms. Rigid constraints were enforced on all bond lengths using the LINCS algorithm.[40] Short-range dispersion interactions were handled using a twin-range cutoff scheme, with interactions between the inner and outer radii (1.0 and 1.2 nm, respectively) updated every 10 time steps. A long-range dispersion correction term was also added to both energy and pressure. The particle-mesh Ewald method[41] with a real-space cutoff of 1.0 nm was applied to deal with long-range electrostatic interactions. Further details concerning the potential calculations were given in a previous publication.[42]

The SPC/E potential,[43] with rigid bonds and bond angle, was employed to model water molecules. This model combines a good description of thermodynamic and structural properties of water with computational tractability[44] and is suitable for studying liquid interfaces involving water.[45,46] In our study, we chose the cationic decyltrimethylammonium bromide (DeTAB) as the surfactant. This molecule is composed of a hydrophilic quaternary ammonium head and a hydrophobic aliphatic tail with 10 carbon atoms. In the presence of a silica source, this surfactant can be used to template the synthesis of MCM-41,[1] the most widely studied PMS material, with nearly cylindrical pores packed in a regular hexagonal arrangement.[4] MCM-41 is most commonly synthesized using a longer chained surfactant (cetyltrimethylammonium bromide). However, simulating the self-assembly of an atomistic model of this surfactant would require time and length scales that are beyond current computational capabilities, whereas previous atomistic simulations of the more tractable shorter-chained DeTAB have been able to describe in detail the formation of several micellar aggregates of this surfactant.[42] The $DeTA^+$ molecule was modeled using a united-atom representation; i.e., all CH_2 and CH_3 groups were represented by a single interaction center, without considering explicit hydrogens. Potential parameters for the head group were taken from Jorgensen and Gao,[47] and parameters for the aliphatic tail were taken from Smit et al.[48] The performance of this model in self-assembly simulations has been shown to be equivalent to that of a more realistic but more computationally expensive all-atom model.[42]

In this work, we aimed to describe the synthesis of a PMS starting from an aqueous solution of DeTAB and a monomeric silica source at high pH. We studied four different silica/surfactant/water solutions: (i) a reference solution composed only of DeTAB and water; (ii) a monomeric solution that contained also neutral and anionic silicic acid monomers, representing the start of the synthesis process before any condensation has taken place; (iii) an oligomeric solution, which contained a distribution of silicate oligomers (dimers, linear and cyclic trimers, and linear, cyclic, and branched tetramers), meant to represent a later stage in the process, after some amount of silica condensation has occurred; (iv) an "exchange solution", in which anionic silica monomers were added to a previously equilibrated DeTAB/water micellar solution, to study the ion exchange between bromide and silicates. In the exchange solution, overall charge neutrality of the system was ensured by adding one tetramethylammonium (TMA) cation per anionic silicic acid monomer (mimicking the experimental addition of TMA silicate to a DeTAB/water solution, as in the work of Firouzi et al.[11]). The TMA cations are essentially equivalent to a $DeTA^+$ molecule without the hydrophobic tail and were modeled using the parameters of Jorgensen and Gao.[47]

Explicit MD simulations of silica condensation are not feasible at the conditions studied in this paper due to the inability of that method to sample the time scales required for the reactions to take place. In order to study the effect of silica condensation, we have simulated a system—the oligomeric solution—in which the silicates are more condensed but where silica condensation is still "frozen". This is a reasonable approximation, given that surfactant self-assembly takes place on a much shorter time scale than the condensation reactions. The relative proportion of each silicate species in the oligomeric solution was thus estimated from NMR characterization studies of silicate solutions,[49] while their degree of deprotonation was calculated from acid−base equilibrium[50] at a pH of 11. In Table 1, we show topology diagrams for each silicate oligomer, as well as their net charges, and relative proportions in the solution. In our notation, we consider that each silicate oligomer is formed

TABLE 1: Structures and Fractions of Silicate Species Included in the Oligomeric Solution

Name	Formula	Charge	Charge/Si	Topology	Mole %[a]	% of Si[b]	Nr. of molecules[c]
SNSI	$Si_2O_7H_5$	-1	-0.5	—	8.4	5.4	4
SI2	$Si_2O_7H_4$	-2	-1	—	12.6	8.1	6
SI3	$Si_3O_{10}H_5$	-3	-1	^	23.9	22.9	12
SI3c	$Si_3O_9H_3$	-3	-1	△	21.5	20.6	10
SI4	$Si_4O_{13}H_6$	-4	-1	~	7.3	9.3	4
SI4c	$Si_4O_{12}H_4$	-4	-1	□	11.2	14.3	5
SI4b	$Si_4O_{12}H_4$	-4	-1	⧋	15.1	19.3	7

[a] Calculated based on the relative proportions of dimers, trimers, and tetramers in silicate solutions obtained from NMR measurements.[49] [b] Calculated from the mole percentage and the total number of Si atoms on each oligomer. [c] Calculated from the percentage of Si and the number of Si atoms on each oligomer, considering a total of 150 Si atoms in the system.

by a combination of connected neutral and anionic fragments, denoted respectively by SN and SI, with each fragment including a central silicon atom and the surrounding oxygen and hydrogen atoms. Thus, a single-charged dimer is labeled as SNSI (one neutral and one anionic fragment), a double-charged dimer is labeled SI2 (two anionic fragments), and so on. We also introduce the letters "c" to denote a cyclic structure and "b" to denote a branched structure. Notice that the solution contains a large proportion of cyclic silicates, in agreement with NMR experiments[49] and ab initio calculations.[51]

Under the alkaline conditions studied here, most silicates are in their deprotonated anionic form.[50] Unfortunately, we are not aware of any available force field that incorporates reliable parameters for soluble anionic silicates. Pereira et al.[52] have developed a force field for soluble neutral silicates based on previous ab initio calculations by Hill and Sauer[53] and on their own density functional theory (DFT) studies on neutral silicates.[54] Their potential parameters were validated against experimental data for pure, liquid silica alkoxides at several temperatures and pressures.[55] Thus, we have adapted the force field of Pereira et al.[52] by modifying some parameters according to our own DFT calculations of anionic silicate species.[51] In particular, the angle bending force constants, the torsional parameters, and the L-J parameters were kept unchanged, while the bond lengths and angles were slightly modified in accordance with our recent DFT geometries (obtained using a larger basis set than that used by Pereira et al.[54]). The major changes implemented were in the values of the point charges, which in our case were obtained by averaging the CHelpG charges[56] computed from the DFT optimization of several neutral and anionic silicate monomers, dimers, trimers, and tetramers.[51] In order to make the silicate force field more general, we considered only 10 atom types: a silicon atom belonging to a neutral fragment (Si_N), a silicon belonging to an anionic fragment (Si_I), an oxygen of a hydroxyl group belonging to a neutral (Oh_N) and to an anionic (Oh_I) fragment, a hydroxyl hydrogen in a neutral (H_N) and in an anionic fragment (H_I), a negatively charged oxygen atom in an anionic fragment (Oc), a bridging oxygen connecting two neutral fragments (Ob_{NN}), a neutral and an anionic fragment (Ob_{NI}), or two anionic fragments (Ob_{II}). The full set of potential parameters for silicates is given in Tables 2−5. It is worth noticing that, despite the different approaches used, our values for the point charges of neutral silicates, shown in Table 2, are not very far from those proposed previously by Pereira et al.[52]

TABLE 2: Intermolecular Parameters for Neutral and Anionic Silicates

atom	mass (au)	σ (nm)	ε (kJ mol^{-1})	q (au)
Si_N	28.086	0.4435	0.3975	1.3292
Si_I	28.086	0.4435	0.3975	1.0801
Oh_N	15.999	0.3462	0.6657	−0.7641
Oh_I	15.999	0.3462	0.6657	−0.7481
H_N	1.008	0.2354	0.4134	0.4318
H_I	1.008	0.2354	0.4134	0.3684
Ob_{NN}	15.999	0.3451	0.6786	−0.6646
Ob_{NI}	15.999	0.3451	0.6786	−0.7120
Ob_{II}	15.999	0.3451	0.6786	−0.7594
Oc	15.999	0.3462	0.6657	−0.9410

TABLE 3: Bond Lengths (in nm) for Neutral and Anionic Silicates

bond	length
Si_N-O^a	0.165
Si_I-O^a	0.169
O^a-H^b	0.097
Si_I-Oc	0.158

[a] Any oxygen atom except Oc. [b] Any hydrogen atom.

Each solution studied contained 150 $DeTA^+$ molecules. In the reference solution, these were neutralized by 150 bromide counterions. The monomeric solution contained, apart from the 150 $DeTA^+$ molecules, 146 SI and 4 SN molecules (as explained above, this SI/SN ratio was calculated from acid−base equilibrium at pH = 11). This corresponds to a surfactant/silica ratio of 1. The oligomeric solution contained the same proportion of neutral and anionic silica fragments as in the monomeric solution, but in the form of the silicates shown in Table 1. In both the monomeric and oligomeric solutions, four bromide ions were also added to neutralize the overall charge of the system.

TABLE 4: Harmonic Angle Potential Parameters for Neutral and Anionic Silicates

angle	θ_0 (deg)	k_θ (kJ mol^{-1} rad^{-2})
$Si_N-Oh_N-H_N$	114.4	103.46
$Si_I-Oh_I-H_I$	109.8	103.46
$Oh_N-Si_N-Oh_N$	109.6	232.96
$Ob^a-Si_N-Oh_N$	109.6	412.62
$Ob^a-Si_N-Ob^a$	109.6	562.47
$Oh_I-Si_I-Oh_I$	104.9	232.96
$Ob^a-Si_I-Oh_I$	104.9	412.62
$Ob^a-Si_I-Ob^a$	104.9	562.47
Oh_I-Si_I-Oc	114.2	232.96
Ob^a-Si_I-Oc	114.2	412.62
$Si_N-Ob^a-Si_N$	135.9	19.52
$Si_N-Ob^a-Si_I$	131.5	19.52
$Si_I-Ob^a-Si_I$	130.3	19.52

[a] Any bridging oxygen atom.

TABLE 5: Ryckaert−Bellemans Torsional Potential Parameters (in kJ mol^{-1}) for Neutral and Anionic Silicates

dihedral	C_0	C_1	C_2	C_3
Oh−Si−Oh−H	14.8473	9.1554	−3.6233	2.0686
Oc−Si−Oh−H	14.8473	9.1554	−3.6233	2.0686
Ob−Si−Oh−H	15.2038	23.8622	−2.5673	−9.8910
Oh−Si−Ob−H	−3.3698	−4.0041	−0.6343	0.0000
Oc−Si−Ob−H	−3.3698	−4.0041	−0.6343	0.0000
Ob−Si−Ob−H	−4.0225	−4.0225	0.0000	0.0000

The starting configurations for the reference, monomeric, and oligomeric solutions were built by randomly dispersing the surfactant, bromide ions, and silicates in an empty cubic box. These configurations were then solvated in SPC/E water by using the coordinates of water molecules in a previously equilibrated pure water box and removing those that overlapped with existing surfactant, bromide, and silicate atoms. The box size was adjusted during the solvation stage in order to obtain configurations with 7500 water molecules for all three solutions. Before the start of the MD runs, the energy of each system was minimized using a steepest descent algorithm to eliminate any short-range contact between atoms. After equilibration, the surfactant concentrations (based on the average system volume) in the reference, monomeric, and oligomeric solutions were respectively 0.867, 0.845, and 0.868 M. An overall density of ~44 mol/L was obtained in the reference, monomeric, and oligomeric solutions, while a value of 39 mol/L was obtained in the exchange solution.

To generate the exchange solution, a different procedure was employed. First, all water molecules were removed from a pre-equilibrated DeTAB/water micellar solution (the last configuration of the reference solution, with 150 DeTAB pairs). Then, 150 SI molecules and 150 TMA cations were randomly dispersed in the box, avoiding overlaps with existing surfactant and bromide atoms. This insertion process was divided in steps consisting of the insertion of 50 molecules, followed by a steepest descent energy minimization. After all SI and TMA molecules were successfully inserted, the total system was resolvated in SPC/E water using the same method as for the other solutions. This yielded a system with 5860 water molecules, since the box size was kept unchanged and additional space was now occupied by SI and TMA molecules. After another steepest descent energy minimization, the MD run was started. After equilibration, the average surfactant concentration in this solution was 0.916 M. It is important to note that the concentration of charged species in the exchange solution is about twice that of the monomeric solution.

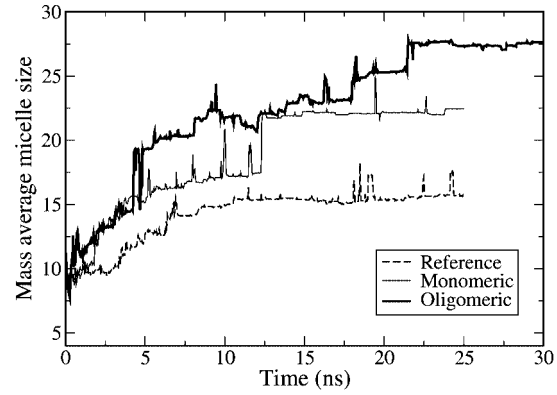

Figure 1. Plot of the mass-average micelle size as a function of simulation time for the reference (dashed line), monomeric (thin line), and oligomeric (thick line) solutions.

An important property that we wish to compute is the distribution of surfactant aggregates in each solution. For that purpose, we identified the individual clusters of surfactants present in each sampled configuration using an adaptation of the Hoshen−Kopelman cluster-counting algorithm.[57] Two surfactant molecules were considered to belong to the same aggregate if any of their last four tail atoms were separated by no more than 0.64 nm (distance close to the first minimum in the radial distribution functions between tail carbon atoms). We have tested this criterion against several other methods and found it to be the most effective.[42] Once the aggregates are identified, we are able to monitor the concentration of clusters of a given size as a function of time. Of these values, the concentration of isolated monomers in solution, $[M_1]$, assumes particular importance. Also important is the mass average micelle size (MS_m), which we calculate by considering as micelles all clusters containing at least five surfactant molecules.[42] We also obtain a measure of the micelle size and shape by calculating the moments of inertia tensor of each aggregate.[42] After diagonalization of this tensor, we obtain the three principal moments of inertia (I_{xx}, I_{yy}, and I_{zz}, ordered from the smallest to the largest) and, from these, the micelle radius of gyration (R_g):

$$R_g = \sqrt{I_{xx} + I_{yy} + I_{zz}} \quad (1)$$

Using R_g and the average micelle size, we can obtain an estimate of the mean surface area per surfactant head group (a), which is a commonly used parameter to describe the mesostructure of surfactant solutions.[58] Finally, we have also monitored the degree of counterion binding, measured as the fraction of ions that are bound to at least one surfactant head group (β). A bromide ion is considered to be bound to a head group if its distance to the surfactant nitrogen atom is below 0.675 nm (the first minimum of the corresponding radial distribution function[42]). Using the same approach, we consider that a silicate ion is bound if the Si−N distance does not exceed 0.72 nm. Using these criteria, we have also calculated the number of bound surfactant molecules per ion (Sb) and the number of bound micelles per ion (Mb).

3. Results and Discussion

3.1. The Monomeric Solution. We begin our discussion by comparing DeTAB self-assembly in our reference aqueous solution with that in the solution containing anionic silica monomers. In Figure 1 we show the evolution of the average cluster size with simulation time for the reference and mono-

TABLE 6: Properties of the Micellar Systems Averaged over the Plateau Regions of Each Simulation Run (Variables Defined in the Text)

property	reference	monomeric	oligomeric	exchange
$\langle MS_m \rangle$	15.5	22.1	27.5	33.0
$[M_1]$ (mol/L)	0.014	0.013	0.026	0.003
I_{xx} (nm^2)	0.282	0.323	0.379	0.438
I_{yy} (nm^2)	0.359	0.404	0.461	0.532
I_{zz} (nm^2)	0.405	0.453	0.515	0.587
R_g (nm)	1.023	1.086	1.164	1.248
a (nm^2)	0.846	0.670	0.620	0.594
β_{Br}	0.610			0.464
Sb_{Br}	1.306			1.380
Mb_{Br}	1.091			1.083
β_{Si}		0.770	0.924	0.766
Sb_{Si}		1.637	4.176	1.821
Mb_{Si}		1.068	1.361	1.060

meric solutions. Comparison of the time evolution of these two solutions reveals that their short-time behavior is rather similar and is characterized by a fast initial stage of surfactant aggregation to form small clusters, followed by an Ostwald ripening process until the system is mostly composed of isolated surfactants and micelles. During the Ostwald ripening process, smaller unstable aggregates dissolve in favor of larger more stable aggregates. This short-time evolution during DeTAB self-assembly has been studied in detail in a previous publication[42] and is not considered further here. It suffices to say that the initial stages of micelle formation are dominated by diffusion-limited monomer aggregation. Thus, it is reasonable to expect that the presence of small silicates will not have a strong effect on the short-time behavior of the system, since they will not provoke significant changes on the mobility of isolated surfactant molecules. In agreement with this reasoning, the curves for the monomeric and reference solutions coincide up to about 1.5 ns. At longer times, however, the situation changes, and the curves begin to diverge. At this stage, growth proceeds mostly by collisions between micelles.[42] These appear to be favored by the presence of silica monomers, leading to a significantly higher average micelle size at the end of the run. This effect is due to a strong interaction between anionic silica monomers and cationic surfactant head groups, as we will demonstrate below. This interaction leads to a more efficient shielding of the head group repulsion, promoting micelle collision and favoring the formation of larger micelles.

As can be seen in Figure 1, both the reference and the monomeric solution runs reach an approximately constant average micelle size after about 13 ns. We calculated several properties of the micellar systems by averaging over all configurations in the plateau regions. Table 6 presents the average values of these properties for all solutions studied. As expected from an analysis of Figure 1, the micelles formed in the monomeric solution possess, on average, more surfactant molecules than those formed in the reference solution. This has been confirmed by visual inspection of snapshots of typical micelles formed in each of these runs, such as those shown in Figure 2. As described in section 2, one can obtain a measure of the micelle size and shape by calculating the moments of inertia tensor for each aggregate. The average values for the diagonal components of this tensor show that micelles in both solutions are nearly spherical, with a slight tendency for a prolate ellipsoid shape (see Figure 2). The average radius of gyration increases when silica monomers are present, reflecting an increase in the mass average micelle size.

More details regarding the increase in micelle size can be obtained by looking at the cluster size distributions (CSDs) for the reference and monomeric solutions, shown in Figure 3. Both CSDs exhibit a first peak for free surfactants and small aggregates (with fewer than four surfactant molecules), separated by a trough from a region corresponding to micellar aggregates. Qualitatively speaking, this shape of the CSD is what we would expect to see in an equilibrated micellar solution. The two systems, however, show some important differences: the reference solution shows a clearly defined micelle peak centered around 15 surfactants, while the CSD for the monomeric solution is rather spiky, with several separate peaks for micelles. More importantly, the micellar region extends up to aggregates with 37 surfactants in the monomeric solution but does not go beyond 22 surfactants in the reference solution. This suggests that the presence of silica monomers is inducing the formation of a population of rather large micelles, which are not present in the reference solution.[33] It may also indicate that the monomeric solution has not yet reached full thermodynamic equilibrium, the implications of which will be discussed below.

The formation of large micelles in the presence of silica can be better understood by examining their structure more closely. In Figure 4, we compare the density profiles measured radially from the micelle center of mass (COM) for micelles of the same size present in the reference and monomeric solutions. Both micelles exhibit a hydrophobic core composed exclusively of surfactant tail atoms (green lines in Figure 4), followed by a well-defined peak for hydrophilic head atoms (purple lines) at the micelle surface. In the reference solution, the positive charge of the surfactant heads is partially compensated by the presence of a rather diffuse layer of bromide counterions (black dashed line) on the outside of the head group layer. In the monomeric solution, the charge compensation is accomplished by the anionic silica monomers (thin red line). These, however, are located predominantly on the *inside* of the head group layer. The presence of this peak for silica monomers causes a reduction of the water density in this region (compare blue lines in Figure 4).

The different location of silicate and bromide counterions relative to the micelle surface is caused by a strong attraction between anionic silicates and cationic surfactant heads. This strong attraction also manifests itself in a higher degree of counterion binding for the monomeric solution. Indeed, the average fraction of bound silica monomers is 0.77, while that of bromide is only 0.61 (see Table 6). The location of the silica monomers within the head group layer allows for these ions to interact with more surfactant heads at the same time. Thus, the average number of surfactants bound to each counterion increases from 1.31 in the reference solution to 1.64 in the monomeric solution. All these observations indicate that silica monomers are more effective at shielding the positive charge at the micelle surface, which brings about a significant decrease in the average area per head group (Table 6). Phenomenological models of surfactant systems argue that, if the average volume of the surfactant tail region and the critical length of the aliphatic tail are the same (this is reasonable, since the structure of the tail region is not affected by the presence of silica; see Figure 4), a lower area per head group decreases the preferred curvature of the aggregates, favoring the formation of larger micelles.[58] This is indeed what we observe in our simulations.

One can analyze counterion binding to DeTAB micelles in even more detail by calculating the fraction of bound ions as a function of micelle size. The results of such calculations are shown in Figure 5 for the reference and monomeric solutions. In the case of the reference solution, we can see that the fraction of bound bromide ions is practically independent of micelle size,

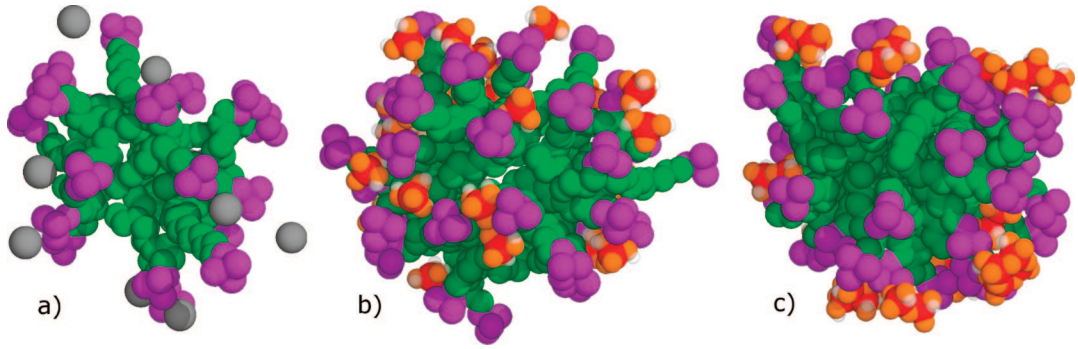

Figure 2. Snapshots of typical micelles observed during the self-assembly simulations of (a) reference solution, (b) monomeric solution, and (c) oligomeric solution. Surfactant tail atoms are represented by green spheres, head atoms are purple, bromide ions are gray, silicon atoms are red, silicate oxygens are orange, and hydrogens are white transparent spheres. Surrounding water molecules have been removed for clarity.

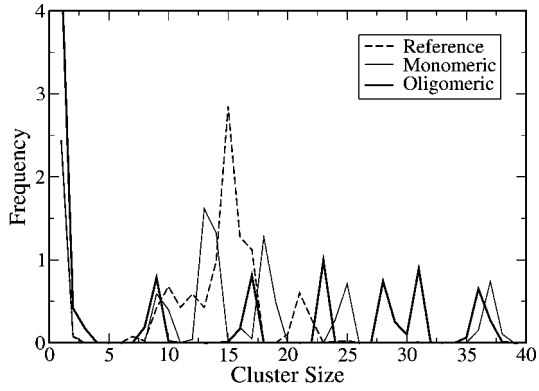

Figure 3. Cluster size distributions for the reference (dashed line), monomeric (thin line), and oligomeric (thick line) solutions.

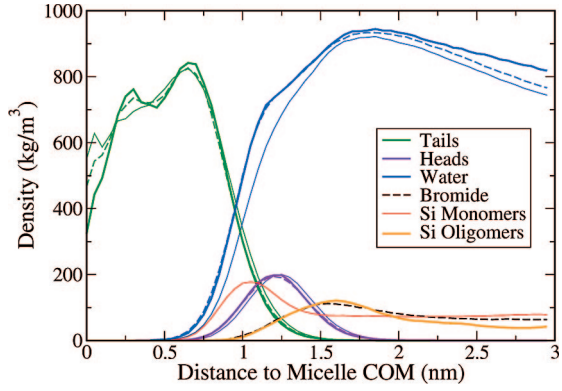

Figure 4. Comparison between the density profiles of micelles containing 17 or 18 surfactant molecules, formed in the reference (dashed lines), monomeric (thin lines), and oligomeric (thick lines) solutions. The different types of atoms are color coded as follows: green, tail atoms; purple, heads; blue, water; black, bromide; red, silica monomers; orange, silica oligomers.

fluctuating around the average value given in Table 6. The monomeric solution, however, shows a markedly different behavior. In this solution, one can distinguish between small micelles, with a degree of counterion binding of ~0.6, and large micelles, with much higher degrees of binding. Thus, one can clearly speak in terms of two distinct micelle populations in the monomeric solution: small micelles, similar to their counterparts in aqueous DeTAB solutions, coexisting with large micelles with a much higher silica concentration at their surface.

3.2. The Oligomeric Solution. The distribution of silicate species in solution is mostly governed by silica condensation equilibrium,[50] according to the reaction:

$$\equiv Si{-}OH + HO{-}Si\equiv \rightleftarrows \equiv Si{-}O{-}Si\equiv + H_2O \qquad (2)$$

The presence of a high concentration of silica monomers at the surface of surfactant micelles, as described in the previous section, shifts the equilibrium of reaction 2 to the product side, promoting the formation of larger silicate species. Thus, we may expect these larger silicates to be present in the PMS synthesis solution at a later stage of the process. To emulate this scenario, we have studied surfactant self-assembly in a solution containing a distribution of anionic silica oligomers, as described in section 2. The evolution of the mass average micelle size as a function of time for this oligomeric solution is also shown in Figure 1. As we can see, the average micelle size at the end of the simulation run is higher than in the monomeric solution and much higher than in the reference solution. This indicates that silica oligomers are even more effective than monomers at promoting the formation of larger micelles.

The CSD for the oligomeric solution (Figure 3) is qualitatively similar to that of the monomeric solution, except for the fact

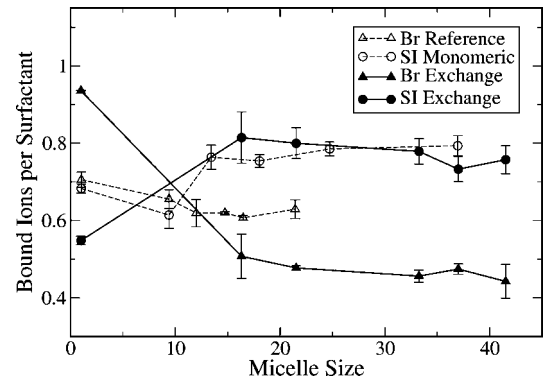

Figure 5. Number of bound ions per surfactant molecule as a function of micelle size for the reference solution (open triangles), monomeric solution (open circles), and exchange solution (Br, filled triangles; SI, filled circles). The lines are guides to the eye.

that a higher proportion of large micelles exist in the former. Micelles formed in the oligomeric solution are still virtually spherical, with a larger gyration radius than in the other two solutions (see Figure 2c and Table 6). The structure of the tail group core and the head group layer is almost identical to those of the reference and monomeric solutions (Figure 4). Once again, the main difference in micelle structure is related to the position of the counterions. In the oligomeric solution, the silica anions are located on the outside of the head group layer, in a similar position as the bromide ions in the reference solution (see thick orange line in Figure 4).

Judging only by the relative location of the counterions, one might have expected the oligomers to behave more like bromide ions and be less efficient at shielding the charge of the surfactant head groups. However, the opposite happens: oligomers are even more effective than monomers and promote the formation of even larger micelles. This effect is most likely caused by the fact that most of the oligomers are multiply charged, which means that negatively charged atoms are much closer to each other in an oligomer than they would be in individual monomers. This proximity increases the local electrostatic potential in the vicinity of the oligomers, enhancing their affinity for cationic head groups. As a consequence, we observe a dramatic increase in the degree of counterion binding for the oligomeric solution (see Table 6)—in fact, almost all oligomeric silicates are bound to at least one surfactant molecule. Thus, silica oligomers are binding even more strongly to surfactant molecules, reducing even further the average area per head group (Table 6) and further promoting an increase in micelle size.

An important stage of the synthesis of MCM-41 and other hexagonally ordered PMS materials seems to be the formation of cylindrical surfactant micelles. In our simulations, however, the shape of the micelles was not significantly affected by the presence of silica (Table 6), and we have not observed the formation of cylindrical micelles. There are three possible reasons for this fact: (i) silica does not induce a sphere-to-rod transition in cationic micellar systems; (ii) our simulations are too short and/or small to observe the transition; (iii) the $DeTA^+$ surfactant is unable to form cylindrical micelles in the range of conditions studied. The first hypothesis is not very likely since experimental studies have provided clear evidence for sphere-to-rod transitions upon silica addition to cationic surfactant solutions.[12,13,16] The second hypothesis can only be tested in an atomistic framework by performing much larger and longer simulations, which are currently beyond available computational resources. The third hypothesis may well be true since we are aware of no experimental studies where $DeTA^+$ forms cylindrical micelles. Thus, because of our choice of surfactant and of limits in computer power, we are currently unable to explore at the molecular level the mechanism by which silica induces a sphere-to-rod transition in surfactant solutions.

Silica monomers are relatively small molecules and are able to fit inside the head group layer without significantly disrupting the structure of the micelle. Silica oligomers, however, are much bulkier and can no longer fit inside the head region. They are therefore pushed to the outside of the micelle surface, where they interact with several surfactants simultaneously. An important consequence of the ability of oligomers to act as multidentate ligands is that they start to interact closely with surfactants on *different* micellar aggregates. This can be clearly seen in Figure 6, where a snapshot of a cross section of the simulation box during the oligomeric run shows silica oligomers bound to two separate micelles. We have quantified the average degree of cross-micelle binding and present the calculated values in Table 6. From these results, we can see that bromide ions and silica monomers are typically bound to a single micelle, whereas silica oligomers are connected on average to about 1.36 micelles. As we will discuss below, this ability plays an important role in the synthesis mechanism of PMS materials.

3.3. The Exchange Solution. In this section, we emulate more closely the experimental PMS synthesis process by adding anionic silica monomers to a micellar solution of DeTAB in water, using the procedure described in section 2. In Figure 7a, we show the evolution of the mass average micelle size before (dashed line) and after (full line) the addition of silica. One can see that the addition of silica monomers causes a progressive increase in the average micelle size until a new plateau is reached. The resulting micelle size in the exchange solution is higher than that obtained in the reference, monomeric, and even oligomeric solution. The large difference relative to the monomeric solution is most likely a consequence of the increased ionic strength in the exchange solution, which is known to promote the formation of larger aggregates.[58]

Simultaneously with an increase in micelle size, the addition of silica has another effect—it displaces bromide ions from the

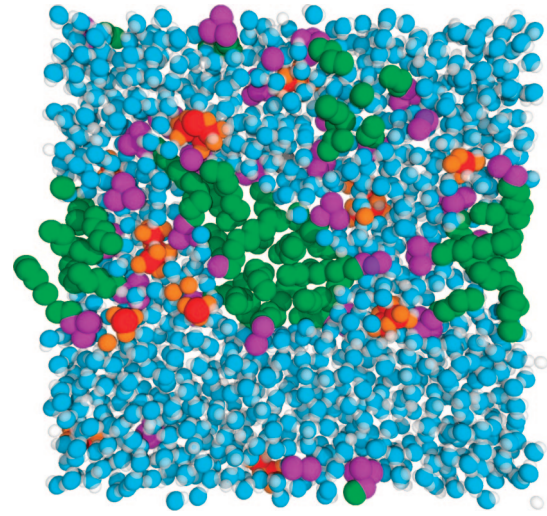

Figure 6. Snapshot of a cross section of the simulation box obtained with the oligomeric solution. Color coding is the same as in Figure 2, except for water oxygens, which are represented as blue spheres. Silica oligomers bound to two different micelles are visible on the left-hand side of the image.

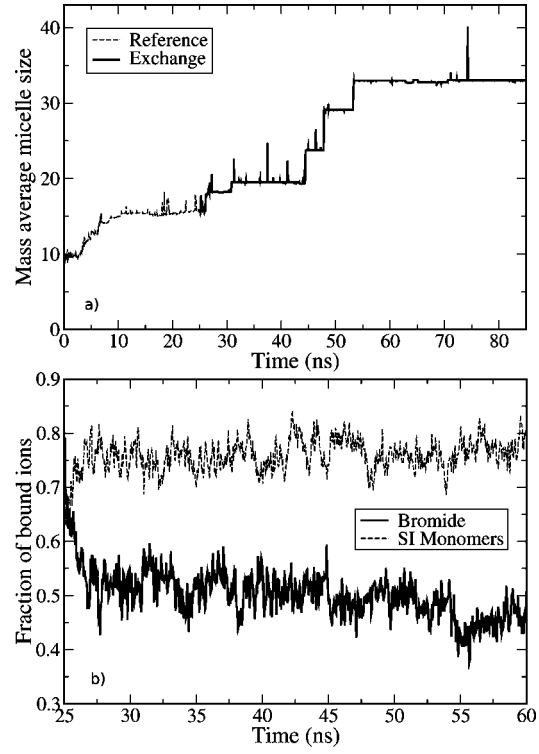

Figure 7. Evolution of (a) the mass average micelle size and (b) the fraction of bound ions in the exchange solution. In (a), the dashed line shows data for the reference solution and the full line shows data after 150 TMA−SI ion pairs were added. In (b), only data after the addition of TMA−SI are shown.

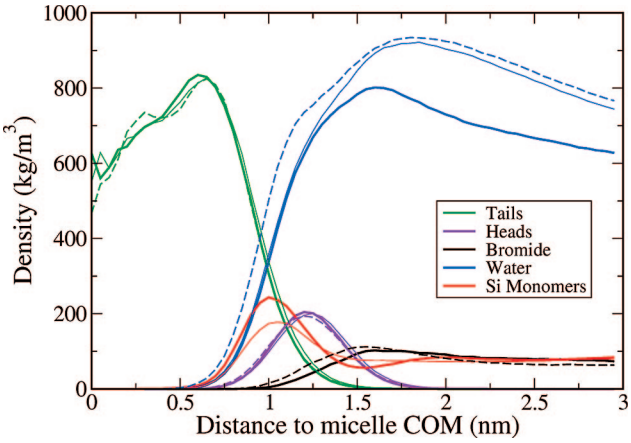

Figure 8. Comparison between the density profiles of micelles containing 17 or 18 surfactant molecules, formed in the reference (dashed lines), monomeric (thin lines), and exchange (thick lines) solutions. The different types of atoms are color coded as in Figure 4.

micelle surface. This displacement can be observed in Figure 7b, where we plot the evolution of the fraction of bound counterions of each type after silica addition. In the first 3 ns of the exchange solution run, the fraction of silicates at the micelle surface increases up to about 0.75, and this is accompanied by a marked decrease in the fraction of bound bromide ions, down to about 0.5. After this relatively fast initial period, further changes in the degree of ionic binding take place much more gradually. It is interesting to compare the average fraction of bound ions in the exchange solution with the corresponding values for the reference and monomeric solutions (see Table 6). Whereas the amount of bound silica is similar in both cases, micelles formed in the exchange solution have significantly less bound bromide than those in the reference solution (i.e., without silica). In fact, about 24% of bromide ions previously bound to $DeTA^+$ micelles at the end of the reference solution run were displaced by the addition of silica. This percentage is within the range of values obtained in the experimental studies of Zana et al.[14,15] and Vautier-Giongo and Pastore.[20]

In Figure 8, we compare the density profiles for micelles of the same size present in the reference, monomeric, and exchange solutions. In all three cases the tail and head peaks are practically identical. In the exchange solution, the silica monomers are located within the head group layer, just as in the monomeric solution, while the bromide ions are on the outside of the micelle, similarly to what is observed in the reference solution. However, the simultaneous presence of bromide and silicate anions causes the latter to protrude even further within the micelle (compare SI peaks for the exchange and monomeric solutions), while the bromides are pushed further outward (compare bromide peaks for the exchange and reference solutions). This effect is most likely due to mutual electrostatic repulsions between both types of anion. The displacement of silica monomers to the inside of the micelle means that they bind even more effectively to surfactant heads, which is translated by an increase in the average number of bound surfactants per silicate anion (Table 6). Finally, the water density profile in the vicinity of the micelle for the exchange solution is very close to its counterpart in the monomeric solution, with a decrease in water density relative to the reference solution being caused by the presence of silica monomers. The lower bulk limiting value for the exchange solution is due to the lower number of water molecules present in this system (see section 2).

More details about the degree of counterion binding can be obtained from Figure 5. We can see that the large micelles present in the exchange solution have virtually the same amount of silica monomers as those in the monomeric solution. The amount of bromide in these micelles, however, is much lower than in corresponding micelles of the reference solution. The different degrees of counterion binding as well as the location of these ions relative to the micelle surface are illustrated in Figure 9 for two micelles of different sizes. Analyzing the curve for Br in the exchange solution, shown in Figure 5, we can see that the depletion in bromide becomes more pronounced as the micelle size increases. These displaced bromide ions migrate to the bulk of the solution, which causes a significant increase in the degree of bromide binding to free surfactant molecules. Thus, one can say that silicate anions interact preferentially with $DeTA^+$ micelles, whereas bromide ions interact preferably with isolated surfactant molecules. A final aspect worth noticing in Figure 5 is the absence of small micelles (with less than 15 surfactants) in the exchange solution, in contrast to their presence in both the reference and the monomeric solutions. Because the exchange simulation starts from a pre-equilibrated micellar solution and is much longer than any of the other solutions, we should expect it to be closer to equilibrium. Thus, our results suggest that the large-micelle population grows at the expense of the small micelles and that beyond a certain stage of the synthesis process the latter will have been completely consumed.

3.4. Mechanistic Implications. Our results from direct simulations of surfactant self-assembly in the presence of silica allow us to draw several conclusions regarding the early stages of the PMS synthesis process. The strong silica−surfactant interaction observed in our simulations promotes an increase in micelle size, in agreement with several experimental observations[12,13,18,23] but in disagreement with others.[14,15] It also causes a significant increase in the local silica concentration at the micelle surface, which facilitates the formation of more condensed silicates. The latter are even more effective than monomers at promoting micelle growth. These observations provide direct evidence to validate previous claims based on the interpretation of experimental results,[5,11,19,22,23,59] thus clearly supporting a cooperative PMS synthesis mechanism based on silica−surfactant interactions.

Furthermore, our simulations of the exchange solution show that the addition of anionic silica to a micellar solution causes the displacement of about 25% of bromide ions previously bound to the surface of micelles, in agreement with experimental studies.[14,15,20] It was argued in those studies that these rather low percentages of bromide displacement implied that silicates did not adsorb substantially on the micelle surface, thus arguing against the CT mechanism proposed by Firouzi et al.[8,11] and supporting a mechanism based on interaction between silicates and free surfactant molecules.[15] It should be noted, however, that the extent of silica adsorption was not measured directly in those studies.[14,15,20] In contrast, our simulations demonstrate that a significant amount of silica does adsorb strongly on the surface of the micelles, coexisting with some previously bound bromide ions. Our results are in excellent agreement with the conclusions of a recent experimental study by Baute et al.[24] and support a cooperative templating mechanism that involves interactions of silicates with micelles.

As silicates condense in the vicinity of the micelle, they move from a location on the inside of the head group layer to the

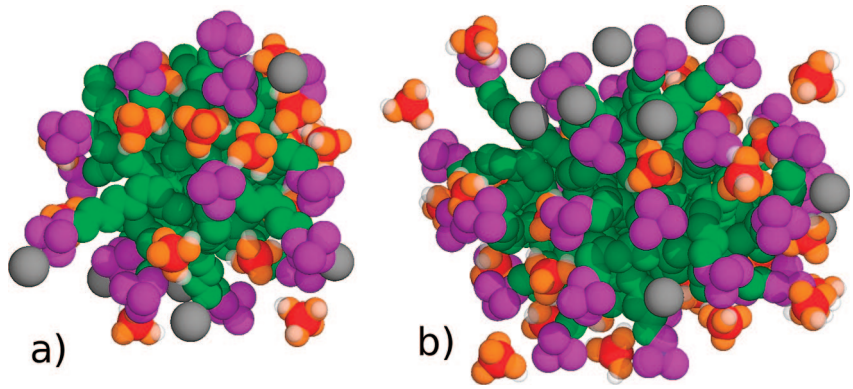

Figure 9. Snapshots of typical micelles observed during the simulations of the exchange solution. Micelle sizes are (a) 21 surfactants and (b) 33 surfactants. Color coding is the same as in Figure 2.

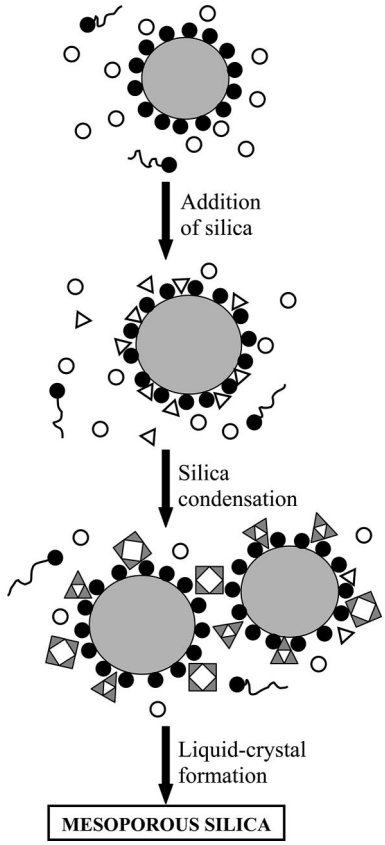

Figure 10. Diagram depicting the proposed mechanism for the early stages of PMS synthesis. Surfactant heads are represented by black circles, bromide counterions are the white circles, micellar hydrophobic cores are depicted by large gray circles, silica monomers are the white triangles, and silica oligomers are represented as arrangements of gray triangles. The process starts from a micellar solution of surfactants and counterions, to which silica is added; silica monomers adsorb on the surface of micelles, increasing their size; the local increase in silica concentration promotes condensation; more condensed silicates further increase micelle size and promote micellar aggregation; micellar aggregates eventually precipitate, giving rise to a liquid-crystal phase.

outside of the micelle. This allows them to interact closely with surfactant molecules belonging to different micelles. The scenario observed in our simulations is in remarkable agreement with the recent experimental study of Baute et al.[24] These authors performed EPR studies of a silica-bound probe and concluded that silica moved to the outside of the micelle upon progressive condensation, leading to the formation of a fluid water/silica layer surrounding several micelles. The intermicelle interactions caused by the presence of large multiply charged anionic silicates will most likely lead to the formation of a separate phase, consisting of aggregates of micelles. Such condensed phases were indeed observed in many experimental investigations of the PMS synthesis mechanism.[8,11,16−19,60,61]

On the basis of our simulation work and of the experimental studies mentioned above, we propose that the mechanism of PMS synthesis starting from a monomeric silica source and a cationic surfactant solution at high pH proceeds as follows (Figure 10), after addition of silica to the surfactant solution: (i) significant adsorption of silicates at the micelle surface, causing some previously bound bromide ions to be displaced to the bulk solution; (ii) micelle growth promoted by a strong silica−surfactant interaction; (iii) silica condensation favored by the increase in local concentration of silica at the micelle surface; (iv) further micelle growth caused by efficient charge dispersion by multiply charged oligomers, which move away from the core of the micelle; (v) binding of multiply charged silicates to different micelles, promoting intermicelle aggregation; (vi) precipitation of a concentrated phase of aggregated micelles surrounded by silica; (vii) further condensation and dehydration leading to the development of the PMS material.

4. Conclusions

In this paper, we have presented a detailed account of our atomistic simulations of cationic surfactant self-assembly in the presence of anionic silica. This approach enabled us to probe the early stages of the synthesis of surfactant-templated periodic mesoporous silica materials at the molecular level and provide an answer to several unresolved issues pertaining to the PMS synthesis mechanism. Our results clearly show that silicates interact strongly with surfactant head groups and promote an increase in micelle size. This interaction takes place preferentially at the micelle surface, rather than with isolated surfactants, causing some displacement of bromide counterions. Furthermore, as silicate species condense to form multiply charged oligomers, they induce micellar aggregation. These observations identify the crucial role played by silicates in determining the final mesostructure of the material and emphasize the cooperative nature of the synthesis mechanism, as illustrated schematically in Figure 10.

Despite the achievements reported above, the atomistic simulation study presented here suffers from an obvious drawback—the limitation in accessible time and length scales. As such, we cannot yet shed any light on the processes taking place at later stages of the synthesis, such as phase separation and liquid-crystal formation. In particular, we are unable to

observe shape transitions from spherical to cylindrical micelles, nor are we able to discriminate whether this takes place before or after micellar aggregation and phase separation. Given the limitations of current computers, these questions may only be addressed at present using more coarse-grained models. Nevertheless, atomistic simulations like the ones presented in this paper may be extremely useful in the development of such models. If successful, this modeling strategy might ultimately lead to a complete understanding of the entire PMS synthesis process.

Acknowledgment. The authors thank the British Council/Conselho de Reitores das Universidades Portuguesas for support through the "Treaty of Windsor Programme" and Acção Integrada Luso-Britânica n. B-11/08. M.J. also acknowledges Associação Luso-Britânica do Porto for a Prof. João Cabral Scholarship.

References and Notes

(1) Beck, J. S.; Vartuli, J. C.; Roth, W. J.; Leonowicz, M. E.; Kresge, C. T.; Schmitt, K. D.; Chu, C. T. W.; Olson, D. H.; Sheppard, E. W.; McCullen, S. B.; Higgins, J. B.; Schlenker, J. L. *J. Am. Chem. Soc.* **1992**, *114*, 10834.

(2) Raman, N. K.; Anderson, M. T.; Brinker, C. J. *Chem. Mater.* **1996**, *8*, 1682.

(3) Ying, J. Y.; Mehnert, C. P.; Wong, M. S. *Angew. Chem., Int. Ed.* **1999**, *38*, 56.

(4) Chen, C. Y.; Li, H. X.; Davis, M. E. *Microporous Mater.* **1993**, *2*, 17.

(5) Monnier, A.; Schüth, F.; Huo, Q.; Kumar, D.; Margolese, D.; Maxwell, R. S.; Stucky, G. D.; Krishnamurty, M.; Petroff, P.; Firouzi, A.; Janicke, M.; Chmelka, B. F. *Science* **1993**, *261*, 1299.

(6) Vartuli, J. C.; Schmitt, K. D.; Kresge, C. T.; Roth, W. J.; Leonowicz, M. E.; McCullen, S. B.; Hellring, S. D.; Beck, J. S.; Schlenker, J. L.; Olson, D. H.; Sheppard, E. W. *Chem. Mater.* **1994**, *6*, 2317.

(7) Huo, Q.; Margolese, D.; Ciesla, U.; Demuth, D. G.; Feng, P.; Gier, T. E.; Sieger, P.; Firouzi, A.; Chmelka, B. F.; Schüth, F.; Stucky, G. D. *Chem. Mater.* **1994**, *6*, 1176.

(8) Firouzi, A.; Kumar, D.; Bull, L. M.; Besier, T.; Sieger, P.; Huo, Q.; Walker, S. A.; Zasadzinski, J. A.; Glinka, C.; Nicol, J.; Margolese, D.; Stucky, G. D.; Chmelka, B. F. *Science* **1995**, *267*, 1138.

(9) Chen, C. Y.; Burkett, S. L.; Li, H. X.; Davis, M. E. *Microporous Mater.* **1993**, *2*, 27.

(10) Attard, G. S.; Glyde, J. C.; Göltner, C. G. *Nature (London)* **1995**, *378*, 366.

(11) Firouzi, A.; Atef, F.; Oertli, A. G.; Stucky, G. D.; Chmelka, B. F. *J. Am. Chem. Soc.* **1997**, *119*, 3596.

(12) Lee, Y. S.; Surjadi, D.; Rathman, J. F. *Langmuir* **1996**, *12*, 6202.

(13) Albuquerque, A.; Vautier-Giongo, C.; Pastore, H. E. *J. Colloid Interface Sci.* **2005**, *284*, 687.

(14) Zana, R.; Frasch, J.; Soulard, M.; Lebeau, B.; Patarin, J. *Langmuir* **1999**, *15*, 2603.

(15) Frasch, J.; Lebeau, B.; Soulard, M.; Patarin, J.; Zana, R. *Langmuir* **2000**, *16*, 9049.

(16) Regev, O. *Langmuir* **1996**, *12*, 4940.

(17) Galarneau, A.; Di Renzo, F.; Fajula, F.; Mollo, L.; Fubini, B.; Ottaviani, M. F. *J. Colloid Interface Sci.* **1998**, *201*, 105.

(18) Sadasivan, S.; Fowler, C. E.; Khushalani, D.; Mann, S. *Angew. Chem., Int. Ed.* **2002**, *41*, 2151.

(19) Beurroies, I.; Ågren, P.; Büchel, G.; Rosenholm, J. B.; Amenitsch, H.; Denoyel, R.; Lindén, M. *J. Phys. Chem. B* **2006**, *110*, 16254.

(20) Vautier-Giongo, C.; Pastore, H. E. *J. Colloid Interface Sci.* **2006**, *299*, 874.

(21) Zhang, J.; Luz, Z.; Goldfarb, D. *J. Phys. Chem. B* **1997**, *101*, 7087.

(22) Zhang, J.; Goldfarb, D. *Microporous Mesoporous Mater.* **2001**, *48*, 143.

(23) Zhang, J.; Carl, P. J.; Zimmermann, H.; Goldfarb, D. *J. Phys. Chem. B* **2002**, *106*, 5382.

(24) Baute, D.; Frydman, V.; Zimmermann, H.; Kababya, S.; Goldfarb, D. *J. Phys. Chem. B* **2005**, *109*, 7807.

(25) Patarin, J.; Lebeau, B.; Zana, R. *Curr. Opin. Colloid Interface Sci.* **2002**, *7*, 107.

(26) Bhattacharya, A.; Mahanti, S. D. *J. Phys.: Condens. Matter* **2001**, *13*, 1413.

(27) Siperstein, F. R.; Gubbins, K. E. *Mol. Simul.* **2001**, *27*, 339.

(28) Siperstein, F. R.; Gubbins, K. E. *Langmuir* **2003**, *19*, 2049.

(29) Patti, A.; Mackie, A. D.; Siperstein, F. R. *Langmuir* **2007**, *23*, 6771.

(30) Patti, A.; Siperstein, F. R.; Mackie, A. D. *J. Phys. Chem. C* **2007**, *111*, 16035.

(31) Schumacher, C.; Gonzalez, J.; Wright, P. A.; Seaton, N. A. *J. Phys. Chem. B* **2006**, *110*, 319.

(32) Gov, N.; Borukhov, I.; Goldfarb, D. *Langmuir* **2006**, *22*, 605.

(33) Jorge, M.; Gomes, J. R. B.; Cordeiro, M. N. D. S.; Seaton, N. A. *J. Am. Chem. Soc.* **2007**, *129*, 15414.

(34) Berendsen, H. J. C.; van der Spoel, D.; van Drunen, R. *Comput. Phys. Commun.* **1995**, *91*, 43.

(35) Lindahl, E.; Hess, B.; van der Spoel, D. *J. Mol. Model.* **2001**, *7*, 306.

(36) Hockney, R. W.; Goel, S P J. *J. Comput. Phys.* **1974**, *14*, 148.

(37) Nosé, S. *Mol. Phys.* **1984**, *52*, 255.

(38) Hoover, W. G. *Phys. Rev. A* **1985**, *31*, 1695.

(39) Parrinello, M.; Rahman, A. *J. Appl. Phys.* **1981**, *52*, 7182.

(40) Hess, B.; Bekker, H.; Berendsen, H. J. C.; Fraaije, J. G. E. M. *J. Comput. Chem.* **1997**, *18*, 1463.

(41) Essman, U.; Perela, L.; Berkowitz, M. L.; Darden, T.; Lee, H.; Pedersen, L. G. *J. Chem. Phys.* **1995**, *103*, 8577.

(42) Jorge, M. *Langmuir* **2008**, *24*, 5714.

(43) Berendsen, H. J. C.; Grigera, J. R.; Straatsma, T. P. *J. Phys. Chem.* **1987**, *91*, 6269.

(44) Boulougouris, G. C.; Economou, I. G.; Theodorou, D. N. *J. Phys. Chem. B* **1998**, *102*, 1029.

(45) Jorge, M.; Cordeiro, M. N. D. S. *J. Phys. Chem. C* **2007**, *111*, 17612.

(46) Jorge, M.; Cordeiro, M. N. D. S. *J. Phys. Chem. B* **2008**, *112*, 2415.

(47) Jorgensen, W. L.; Gao, J. *J. Phys. Chem.* **1986**, *90*, 2174.

(48) Smit, B.; Karaborni, S.; Siepmann, J. I. *J. Chem. Phys.* **1995**, *102*, 2126.

(49) Knight, C. T. G. *Zeolites* **1990**, *10*, 140.

(50) Ščík, J.; McCormick, A. V. *AIChE J.* **1997**, *43*, 2773.

(51) Gomes, J. R. B.; Cordeiro, M. N. D. S.; Jorge, M. *Geochim. Cosmochim. Acta* **2008**, *72*, 4421.

(52) Pereira, J. C. G.; Catlow, C. R. A.; Price, G. D. *J. Phys. Chem. A* **2002**, *106*, 130.

(53) Hill, J.-R.; Sauer, J. *J. Phys. Chem.* **1994**, *98*, 1238.

(54) Pereira, J. C. G.; Catlow, C. R. A.; Price, G. D. *J. Phys. Chem. A* **1999**, *103*, 3252.

(55) Pereira, J. C. G.; Catlow, C. R. A.; Price, G. D. *J. Phys. Chem. A* **2001**, *105*, 1909.

(56) Breneman, C. M.; Wiberg, K. B. *J. Comput. Chem.* **1990**, *11*, 361.

(57) Hoshen, J.; Kopelman, R. *Phys. Rev. B* **1976**, *14*, 3438.

(58) Israelachvili, J. N. *Intermolecular and Surface Forces*; Academic Press: London, UK, 1985.

(59) Cheng, C. F.; Luan, Z.; Klinowski, J. *Langmuir* **1995**, *11*, 2815.

(60) Flodström, K.; Wennerström, H.; Alfredsson, V. *Langmuir* **2004**, *20*, 680.

(61) Ruthstein, S.; Schmidt, J.; Kesselman, E.; Talmon, Y.; Goldfarb, D. *J. Am. Chem. Soc.* **2006**, *128*, 3366.

JP806686W